第37卷第3期
2021年3月

无 机 化 学 学 报
CHINESE JOURNAL OF INORGANIC CHEMISTRY

Vol.37 No.3
516-524

$LiBa_{0.95-y}BO_3$:$0.05Tb^{3+}$,yBi^{3+}荧光粉的制备及荧光性质

鲁 雅[1] 张敏芝[2] 梁刚锋[1] 李春霞[2] 赵国良*[,1,2]
([1]浙江师范大学行知学院,金华 321004)
([2]浙江师范大学化学与生命科学学院,金华 321004)

摘要: 以硼酸和碳酸盐为原料,用高温固相法制备了可被(近)紫外光(369、254 nm)有效激发的Tb^{3+}单掺杂$LiBa_{1-x}BO_3$:xTb^{3+}(物质的量分数x=0.02、0.03、0.04、0.05、0.06、0.07)及Bi^{3+}和Tb^{3+}共掺杂$LiBa_{0.95-y}BO_3$:$0.05Tb^{3+}$,yBi^{3+}(物质的量分数y=0.02、0.03、0.04、0.05、0.06、0.07)的2个系列荧光粉,产物的结构和形貌分别用粉末X射线衍射(PXRD)和扫描电子显微镜进行表征。PXRD测定结果表明2个系列的产物均为纯相$LiBaBO_3$。通过对第一系列产物荧光光谱的测定,筛选出发光强度最好的产物,据此确定铽离子的最佳掺杂量;在此基础上制备出铋离子掺杂量不同的第二系列荧光粉。荧光光谱测定的实验结果表明,Tb^{3+}/Bi^{3+}共掺杂的荧光粉的发光强度好于Tb^{3+}单掺杂的荧光粉,这说明Bi^{3+}对Tb^{3+}有敏化作用;而且随着Bi^{3+}掺杂量的增加,产物的荧光强度表现出先增加后减小的趋势,当Bi^{3+}的掺杂量y=0.03时,产物的荧光强度达到最大。Bi^{3+}和Tb^{3+}之间存在偶极-四极相互作用而进行能量传递。系列荧光粉的CIE坐标显示其发光颜色在一定程度上呈现出由绿色光到白光的渐变趋势。

关键词: 硼酸盐; 共掺杂; 铽; 铋; 荧光粉; 发光性质
中图分类号: O482.31; TQ422 **文献标识码:** A **文章编号:** 1001-4861(2021)03-0516-09
DOI: 10.11862/CJIC.2021.066

Preparation and Fluorescent Properties of $LiBa_{0.95-y}BO_3$:$0.05Tb^{3+}$,yBi^{3+}

LU Ya[1] ZHANG Min-Zhi[2] LIANG Gang-Feng[1] LI Chun-Xia[2] ZHAO Guo-Liang*[,1,2]
([1]*Xingzhi College, Zhejiang Normal University, Jinhua, Zhejiang* 321004, *China*)
([2]*College of Chemistry and Life Science, Zhejiang Normal University, Jinhua, Zhejiang* 321004, *China*)

Abstract: Two series of phosphors of Tb^{3+} single doped $LiBa_{1-x}BO_3$:xTb^{3+} (molar fraction x=0.02, 0.03, 0.04, 0.05, 0.06, 0.07) and Bi^{3+}/Tb^{3+} co-doped $LiBa_{0.95-y}BO_3$:$0.05Tb^{3+}$,yBi^{3+} (molar fraction y=0.02, 0.03, 0.04, 0.05, 0.06, 0.07) of which can be effectively excited by (near) ultraviolet at 369, 254 nm light were prepared by high temperature solid state reaction from boric acid and carbonates. The structures and morphology of the samples were characterized by powder X-ray diffraction (PXRD) and scanning electron microscopy. PXRD measurement shows that the products of the two series are pure phase $LiBaBO_3$. By measuring the fluorescent spectra of the first series of products, the product with the best luminescent intensity was screened out, and the optimal doping amount of Tb^{3+} was determined accordingly; on this basis, the second series of phosphors with different doping amounts of Bi^{3+} were prepared. The experimental results of fluorescent spectra show that the luminescent intensity of Tb^{3+}/Bi^{3+} co-doped phosphors was better than that of Tb^{3+} single-doped phosphors, indicating that Bi^{3+} sensitizes to Tb^{3+}; the fluorescent intensity of the products increased first and then decreased with the increase of Bi^{3+} content, and the luminescence intensity of the products reached the maximum when the doped molar fraction y of Bi^{3+} was 0.03. The energy transfer from Bi^{3+} to Tb^{3+} ions is attributed to the dipole-quadrupole interaction. The CIE chromaticity coordinates of the phosphors show that the luminescent color exhibited a gradual trend from green to white in some degree.

Keywords: borate; co-doped; terbium; bismuth; phosphor; fluorescent property

收稿日期:2020-09-20。收修改稿日期:2021-01-13。
国家自然科学基金(No.51872263)资助。
*通信联系人。E-mail:sky53@zjnu.cn

0 Introduction

As well known, the generation of *f-f* and *f-d* transitions of rare earth ions can absorb or emit electromagnetic radiation of various wavelengths from ultraviolet to near-infrared region, so that rare earth luminescent materials exhibit extremely rich luminescent properties. In fact, the 4*f* transition of rare earth ions is forbidden, and it is relatively inefficient to directly excite rare earth ions. By introducing a low concentration of rare earth ions into the host lattice of the matrix, an inorganic material with ideal luminescence properties can finally be obtained. Among rare earth-doped inorganic materials, the matrix can provide a relatively stable structural environment for the luminescence center (rare earth ion), and compared with the luminescence center (rare earth ion), other co-doped or some matrix materials even have a higher absorption coefficient, so that energy can be effectively transferred to rare earth ions. Compared with lanthanide complexes, quantum dots and organic dyes, inorganic materials doped with rare earth ions have many advantages such as large Stokes shift, high chemical/photochemical stability, sharp emission spectra, long life and low toxicity. Therefore, there are very rich applications and broad research prospects in the fields of displays, sensors, solid-state lasers, biomedicine and so on[1-11].

LEDs have been widely used as indicators, decorative lights, backlights, traffic lights, *etc*. In recent years, the color rendering and brightness of LEDs have been continuously improved. Its significant advantages and broad application prospects make it a research focus at home and abroad. In terms of core technology, phosphor, as an important part of LED, is considered to be a prerequisite for display and lighting functions and success[12]. In combination with the current reality, in the research of phosphors, it is urgent to develop new types of luminescent materials that have long lifespan, high luminous efficiency and can be excited by blue or near ultraviolet LED chips.

In recent decades, researchers have widely developed various types of matrix LED phosphors, mainly including silicate, aluminate, borate, tungsten/molybdate, sulfide, and nitrogen (oxygen) compounds. However, the emission peaks of silicate-based phosphors are relatively narrow, and the color rendering effect of white light after packaging the LED is not good; while the aluminate-based phosphors have high calcination temperature, poor moisture resistance, poor oxidation resistance and single comparable substrates are difficult to prepare and have many other shortcomings; the synthesis cost of nitrogen (oxygen) compounds is high, and the preparation process is complicated, which makes it difficult to realize industrialization.

Borate-based phosphors can be used as a good kind of luminescent matrix materials of rare earth element doped due to their high optical damage threshold and fluorescence efficiency, wide light transmission area, simple preparation process, low synthesis temperature and good thermal stability[13-21]. Scholars at home and abroad have studied many single-doped or multi-doped borate-based phosphors, such as $LiBaBO_3$：Tb^{3+}[22], $Sr_2B_2O_5$：Tb^{3+}, Li^+[23], $NaSrB_5O_9$：Eu^{3+}[24], $Li_6Gd(BO_3)_3$：Tb^{3+}/Bi^{3+}, Eu^{3+}[25], $KBaY(BO_3)_2$：Ce^{3+}, Tb^{3+}, Eu^{3+}[26], $NaSrBO_3$：Ce^{3+}, Sm^{3+}, Tb^{3+}[27], $KSr_4(BO_3)_3$：Dy^{3+}, Tb^{3+}[28], $Sr_3Y_2(BO_3)_4$：Dy^{3+}[29], $Li_6M(BO_3)_3$ (M=Y, Gd)：Eu^{3+}[30], $Li_4Ca(BO_3)_2$：Sm^{3+}[31], $LiBaBO_3$：Eu^{3+}, Bi^{3+}[32], $LiBaBO_3$：Ce^{3+}/Tb^{3+}[33].

Nevertheless, there is still a large space for the research of borate phosphors. In this paper, we report the synthesis of two series of borate-based phosphors $LiBa_{1-x}BO_3$：xTb^{3+} and $LiBa_{0.95-y}BO_3$：$0.05Bi^{3+}$,yTb^{3+}. The crystalline phase structure and microscopic morphology of the phosphor were characterized by powder X-ray diffraction (PXRD) and scanning electron microscopy (SEM), and the luminescence properties of the samples were tested. The mechanism of concentration quenching and energy transfer during the luminescence process of the samples were analyzed and discussed. The product with the best luminescent intensity was screened out by measuring the fluorescent spectrum of the first series of phosphors, thus the optimum doping amount of Tb^{3+} was determined. On this basis, Bi^{3+} was further doped to investigate the effect of Bi^{3+} on Tb^{3+} sensitization, so as to find luminescent materials with better luminescence performance.

What needs to be explained is although the first series of synthesis and the determination of luminescence performance have been reported in the literature[22], in order to know and master the synthesis process and parameters of the first series, the first series of phosphors were synthesized repeatedly and the corresponding characterization and luminescence performance were performed in this paper. The measurement results show that the sample structure is consistent with the literature, and the doping amount of the activated ion at the maximum luminous intensity is different from the literature. All this is to determine the preparation conditions of the second series.

1 Experimental

1.1 Materials and measurements

All of the reagents employed were analytical grade and used without further purification. The phase composition and structure were determined by PXRD (D8 Advance XRD tester, Cu $K\alpha$, λ=0.154 2 nm, 40 kV, 100 mA, 2θ=10°~80°, the slit width was 6.6 nm). The emission and excitation spectra were measured by a FLS980 fluorescence spectrometer of Edinburgh, UK. All the photoluminescence properties of the phosphors were measured at room temperature. The morphology test was carried out with the S-4800 (5 kV) SEM of Hitachi, Japan. In addition. The elemental composition of the sample was analyzed by energy dispersive spectrometer (EDS, Hitachi S-4800, 15 kV). The processing and fitting of the data were completed through Origin9 software.

1.2 Preparation of the samples

1.2.1 Preparation of $LiBa_{1-x}BO_3:xTb^{3+}$

The starting reactants Li_2CO_3, $BaCO_3$, H_3BO_3, $Tb_2(CO_3)_3\cdot H_2O$ (all materials were analytically pure) were weighed accurately according to the stoichiometric ratio and mixed in an agate mortar. The mixture was grinded continuously at least 0.5 h, then it was transferred into a corundum crucible and pre-calcined at 500 ℃ in a high-temperature box-type resistance furnace at a heating rate of 5 ℃·min^{-1} for 2 h. After slowly cooled to room temperature, it was put in an agate mortar again and grinded continuously for at least 0.5 h. The powders were calcined at 700 ℃ for 2 h, and the $LiBa_{1-x}BO_3:xTb^{3+}$ (molar fraction x=0.02, 0.03, 0.04, 0.05, 0.06, 0.07) phosphors were obtained.

1.2.2 Preparation of $LiBa_{0.95-y}BO_3:0.05Bi^{3+},yTb^{3+}$

The preparation method and process were the same as above, except that the reactant $(BiO)_2CO_3$ (analytical purity) was added, and finally the products $LiBa_{0.95-y}BO_3:0.05Bi^{3+},yTb^{3+}$ (molar fraction y=0.02, 0.03, 0.04, 0.05, 0.06, 0.07) were obtained.

2 Results and discussion

2.1 Series of $LiBa_{1-x}BO_3:xTb^{3+}$

2.1.1 Structure of $LiBa_{1-x}BO_3:xTb^{3+}$

Fig. 1 shows the XRD patterns of the series of $LiBa_{1-x}BO_3:xTb^{3+}$ (x=0.02, 0.03, 0.04, 0.05, 0.06, 0.07) phosphors. The datum agreed well with PDF No. 81-1808 of $LiBaBO_3$, therefore the phase purity is high, and the crystallinity is good, indicating that Tb^{3+} in the sample enters successfully the main lattice, and there is no effect on $LiBaBO_3$. $LiBaBO_3$ belongs to the monoclinic crystal system with $P2_1/n$ space group, which is reported by references[22,33].

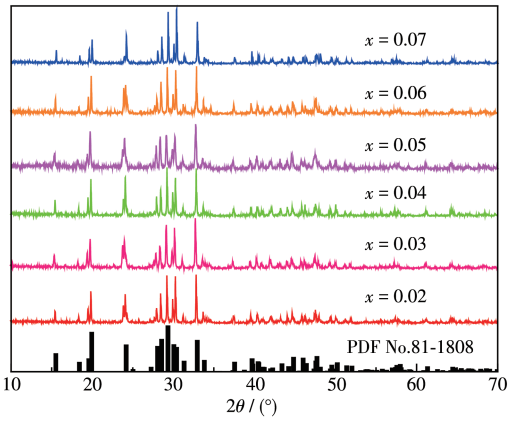

Fig.1 XRD patterns of $LiBa_{1-x}BO_3:xTb^{3+}$ samples

2.1.2 Fluorescent spectra of $LiBa_{1-x}BO_3:xTb^{3+}$

Fig.2 shows the emission and excitation spectra of $LiBa_{1-x}BO_3:xTb^{3+}$ phosphor with Tb^{3+} molar fraction of 0.05. Under the excitation of 369 nm, the emission spectrum exhibited four major emission bands at 488, 544, 583 and 622 nm, which are originated from $^5D_4\rightarrow{}^7F_6$, $^5D_4\rightarrow{}^7F_5$, $^5D_4\rightarrow{}^7F_4$ and $^5D_4\rightarrow{}^7F_3$, characteristics transitions of Tb^{3+} ions, respectively. The strongest one appeared at 544 nm ($^5D_4\rightarrow{}^7F_5$), and its intensity was

much larger than other emission peaks, so the whole sample showed green light emission. The excitation spectrum for 544 nm emission had excitation peak distribution in a range of 200~400 nm, indicating that the phosphor can be effectively excited by near ultraviolet and ultraviolet light. Among them, the broadband excitation peak in a range of 220~280 nm corresponds to the $4f^8 \rightarrow 4f^7 5d^1$ transition of Tb^{3+} ion; the absorption band in a range of 300~400 nm belongs to the $4f \rightarrow 4f$ transition of Tb^{3+} ions; the peaks were located at 318 nm ($^7F_6 \rightarrow {}^5H_6$), 341 nm ($^7F_6 \rightarrow {}^5L_8$), 352 nm ($^7F_6 \rightarrow {}^5L_9$), 359 nm ($^7F_6 \rightarrow {}^5G_6$), 369 nm ($^7F_6 \rightarrow {}^5L_{10}$) and 378 nm ($^7F_6 \rightarrow {}^5D_3$). The strongest excitation peak was located at 369 nm, and the excitation peaks at 378 and 251 nm were also strong. Taking 378, 369 and 251 nm as excitation wavelengths, respectively, the emission spectra of the obtained samples were found to have the same characteristics. Except for the difference in the intensity of the emission peak, the position and shape of the other emission peaks were not significantly different.

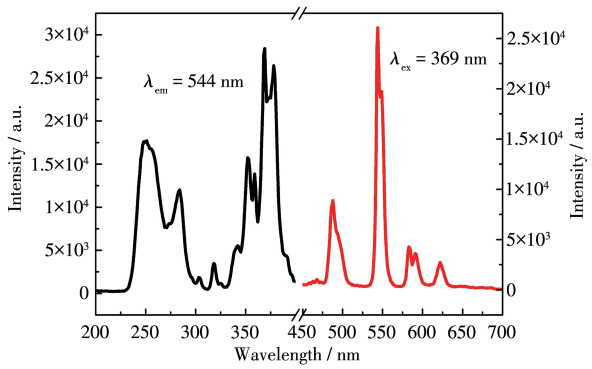

Fig.2　Excitation and emission spectra of $LiBa_{0.95}BO_3$：$0.05Tb^{3+}$ phosphor

The fluorescent spectra of $LiBa_{1-x}BO_3$：xTb^{3+} (x= 0.02, 0.03, 0.04, 0.05, 0.06, 0.07) phosphor samples were very similar. With the gradual increase of doping amount of Tb^{3+}, the luminous intensity at 544 nm gradually increased; when the Tb^{3+} ions doping molar fraction x=0.05, the intensity was the largest, which was different from the results reported in the literature[22]; afterwards, when the doping amount continued to increase, it appeared instead. The tendency of the luminous intensity to weaken is that there is a concentration quenching phenomenon. This phenomenon stems from the fact that as the Tb^{3+} ions were gradually incorporated, the distance between the Tb^{3+} ions in the matrix continued to decrease, and the number of luminescent centers increased accordingly, so the luminous intensity gradually increased, and reached the strongest intensity at the optimal doping amount of Tb^{3+}. However, as the amount of doping continued to increase, the distance between the luminescent centers of Tb^{3+} ions continued to decrease, and the quenching occurred between adjacent Tb^{3+} through non - radiative energy transfer, thus making the luminescent intensity of the phosphor weaked (Fig.3a and 3b).

2.1.3　CIE color chromaticity coordinates of $LiBa_{1-x}BO_3$：xTb^{3+}

Table 1 lists the color chromaticity coordinate values calculated from the emission spectrum of $LiBa_{1-x}BO_3$：xTb^{3+} sample. From this, it can be seen that the emission interval of the phosphor was in the green

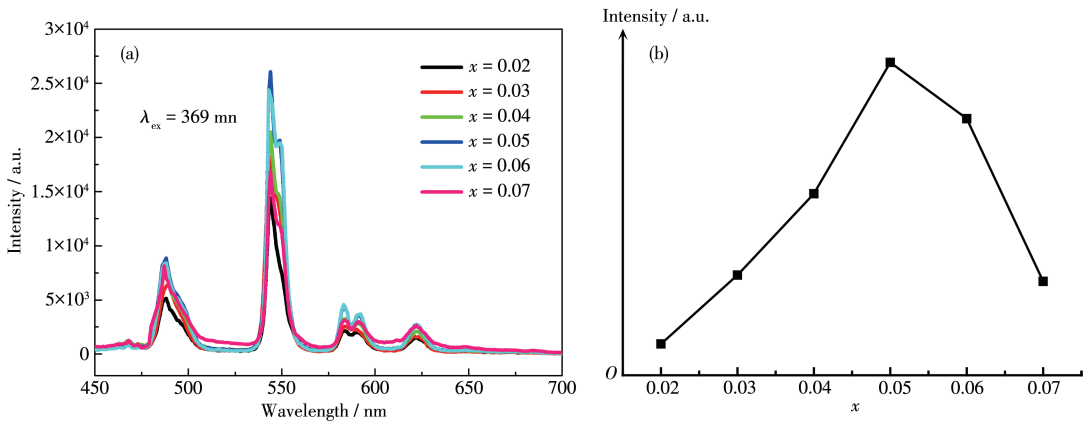

Fig.3　(a) Emission spectra of $LiBa_{1-x}BO_3$：xTb^{3+} phosphors; (b) Relative emission intensity as a function of Tb^{3+} concentration for 544 nm peak

light range. Fig. 4 is a comparison chart of the color coordinates (0.314, 0.535) of $LiBa_{0.95}BO_3$: $0.05Tb^{3+}$ phosphor sample and the green light color coordinates (0.310, 0.595) of the international SMPTE C standard. It can be seen from the figure that the fluorescent pink coordinate of products was close to the standard green color coordinate, and with the change of Tb^{3+} dosage, the change of color chromaticity coordinate was small, indicating that the luminous performance of $LiBa_{1-x}BO_3$:xTb^{3+} phosphor is stable.

Table 1 Chromaticity coordinates of $LiBa_{1-x}BO_3$: xTb^{3+} phosphors excited at 369 nm

x	CIE (x, y)
0.02	0.310, 0.531
0.03	0.304, 0.542
0.04	0.308, 0.546
0.05	0.314, 0.535
0.06	0.320, 0.544
0.07	0.328, 0.532

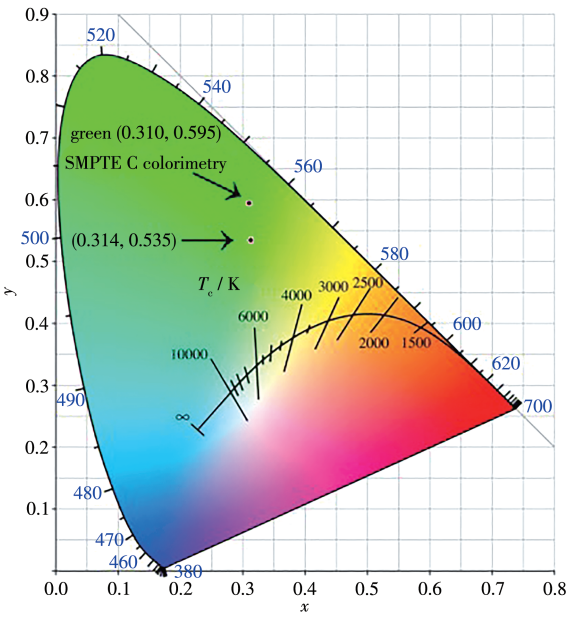

Fig.4 CIE color chromaticity coordinates of $LiBa_{0.95}BO_3$: $0.05Tb^{3+}$ phosphor

2.1.4 SEM of $LiBa_{0.95}BO_3$:$0.05Tb^{3+}$

Fig.5 is a SEM image of $LiBa_{0.95}BO_3$:$0.05Tb^{3+}$ sample at 30 000 times magnification, which shows that the sample was composed of irregular massive agglomerated particles and a large number of needle-like grains on its surface, and the needle-like shape. The length of the grain was 1~2 μm.

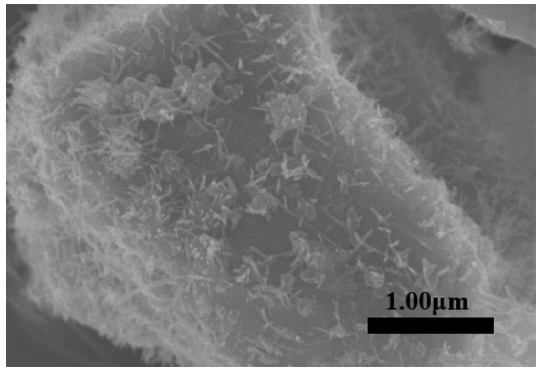

Fig.5 SEM image of $LiBa_{0.95}BO_3$:$0.05Tb^{3+}$ sample

2.2 Series of $LiBa_{0.95-y}BO_3$:$0.05Tb^{3+}$,yBi^{3+}

2.2.1 PXRD of $LiBa_{0.95-y}BO_3$:$0.05Tb^{3+}$,yBi^{3+}

Fig. 6 shows the XRD patterns of phosphor samples with different Bi^{3+} doping amounts, $LiBa_{0.95-y}BO_3$: $0.05Tb^{3+}$, yBi^{3+} (y=0.01, 0.02, 0.03, 0.04, 0.05, 0.06). According to the standard card, $LiBaBO_3$ belongs to the monoclinic system, and the space group is $P2_1/n$. It can be seen from the figure that the positions of the diffraction peaks of the samples are in accordance with the standard card of $LiBaBO_3$ (PDF No. 81 - 1808), which shows that the phase of the prepared series of phosphor samples is pure. It indicates that a small amount of Tb^{3+} and Bi^{3+} ions enter the matrix lattice through calcination, which partially replaces the Ba^{2+} lattice position, and has no obvious effect on the crystal structure of main crystal phase of $LiBaBO_3$.

SEM images at different magnifications and EDS spectrum results of $LiBa_{0.92}BO_3$: $0.05Tb^{3+}$, $0.03Bi^{3+}$ are shown in Fig.7. It can be observed from the figure that

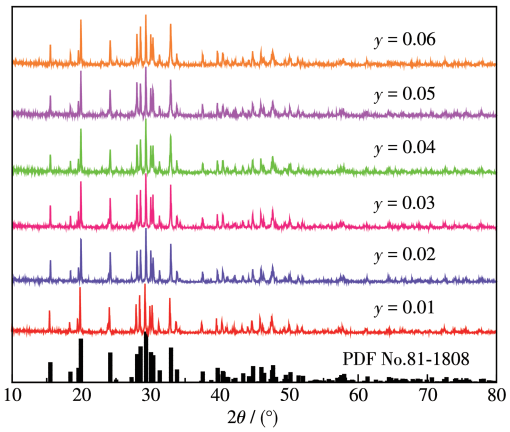

Fig.6 XRD patterns of $LiBa_{0.95-y}BO_3$:$0.05Tb^{3+}$,yBi^{3+} samples

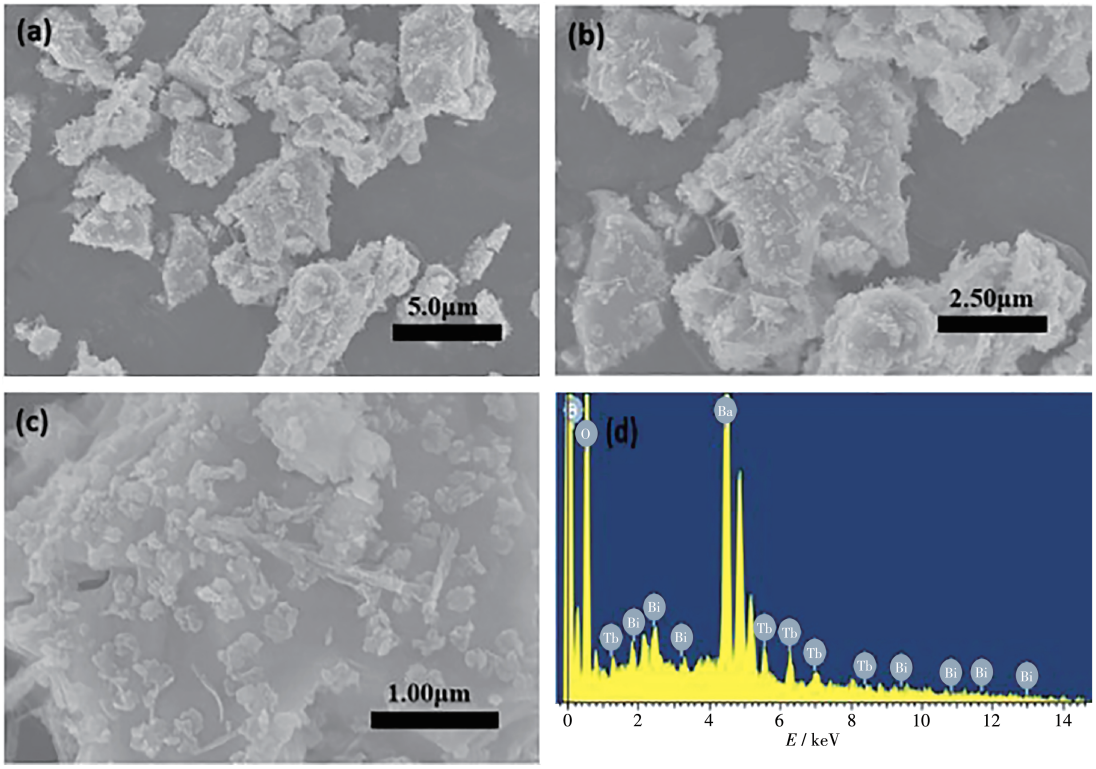

Fig.7　SEM images of $LiBa_{0.92}BO_3$：$0.05Tb^{3+}$, $0.03Bi^{3+}$ sample and corresponding EDS spectrum

the sample was composed of irregular massive agglomerates and a small number of needle-shaped grains. The size of these massive agglomerates was a few microns or less than 1 μm. In order to detect the elemental composition of the sample, the EDS spectrum of the sample was further tested. It can be seen that the chemical composition of this sample included B, O, Tb, Ba, and Bi, indicating that Tb^{3+} and Bi^{3+} are co-doped into the $LiBaBO_3$ matrix. Since the EDS detector was not sensitive to Li, Li did not appear in the EDS spectrum.

2.2.2 Luminescent properties of $LiBa_{0.95-y}BO_3$：$0.05Tb^{3+}$,yBi^{3+}

Fig.8 shows the excitation and emission spectra of $LiBa_{0.94}BO_3$：$0.05Tb^{3+}$，$0.01Bi^{3+}$ phosphor. With 544 nm as the detection wavelength, the excitation spectrum of the sample showed strong absorption peaks in a range of 230~400 nm. The strongest excitation peak was at 254 nm, which belongs to the $4f^8 \rightarrow 4f^7 5d^1$ transition of Tb^{3+} ions; the excitation peaks at 368 nm ($^7F_6 \rightarrow {}^5L_{10}$) and 377 nm ($^7F_6 \rightarrow {}^5D_3$) were also relatively strong, corresponding to $4f \rightarrow 4f$ jump of Tb^{3+} ions. In a range of 300~390 nm, the other narrow excitation peaks of the $4f \rightarrow 4f$ transition of Tb^{3+} ions were 318, 342, 351 and 358 nm, corresponding to $^7F_6 \rightarrow {}^5H_6$, $^7F_6 \rightarrow {}^5L_8$, $^7F_6 \rightarrow {}^5L_9$ and $^7F_6 \rightarrow {}^5G_6$ transition. Taking 254 nm as the excitation wavelength, the main emission peaks of the sample were located at 487, 544, 585 and 621 nm, corresponding to the characteristic $^5D_4 \rightarrow {}^7F_J$ (J=6, 5, 4, 3) transition of Tb^{3+} ion.

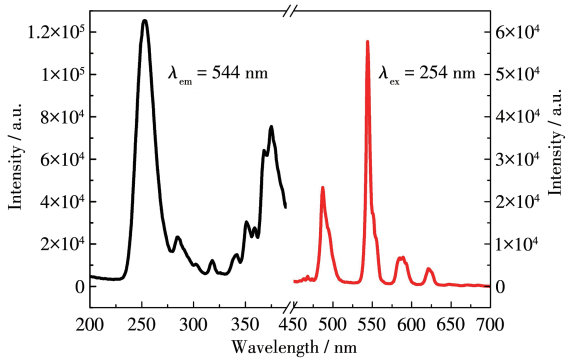

Fig.8　Excitation and emission spectra of $LiBa_{0.94}BO_3$：$0.05Tb^{3+}$, $0.01Bi^{3+}$ phosphor

At the same time, the emission spectra of the samples with Bi^{3+} ion doping amount y=0 and y=0.01 were compared, as shown in Fig.9. We found that after co-doping with a small amount of Bi^{3+} and Tb^{3+} ions, the position and shape of the emission peak hardly

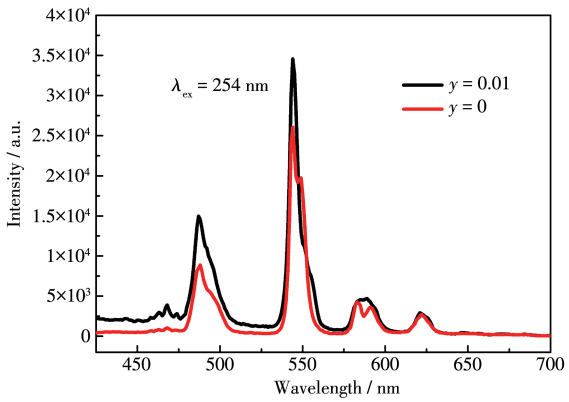

Fig.9 Emission spectra of $LiBa_{0.95-y}BO_3:0.05Tb^{3+},yBi^{3+}$ (y=0, 0.01) phosphors under 254 nm

changed, and the luminous intensity at 544 nm was significantly enhanced, indicating that the doping of Bi^{3+} enhanced the luminous intensity of the activated ion Tb^{3+}.

By changing the doping amount of sensitizing ions Bi^{3+}, the effect of co-doped sensitizing ions and activating ions on the luminescence properties of $LiBa_{0.95-y}BO_3:0.05Tb^{3+},yBi^{3+}$ phosphors was further studied. Fig.10 shows the emission spectra of $LiBa_{0.95-y}BO_3:0.05Tb^{3+},yBi^{3+}$ (y=0.01, 0.02, 0.03, 0.04, 0.05, 0.06) phosphor samples and the luminescence intensity at 544 nm as a function of the amount of doped Bi^{3+}. It can be observed from the figure that the change of doping amount does not affect the position and shape of emission peak of the phosphor, and the emission spectra of all samples included four main emission peaks of 487, 544, 585 and 621 nm. It is worth noting that with the increase of the doping amount y of Bi^{3+} from 0.01 to 0.06, the intensity of the emitted light changes greatly. Initially, when y=0.01~0.03, the luminous intensity of $LiBa_{0.95-y}BO_3:0.05Tb^{3+},yBi^{3+}$ phosphor increased with the increase of the amount of Bi^{3+}. When y=0.03, the luminous intensity was optimal. After that, when the amount of Bi^{3+} ions added further increased, the luminous intensity decreased, which shows that the sensitivity of Bi^{3+} to Tb^{3+} depends on the concentration of Bi^{3+} ions. In this process, it may be that a small amount of Bi^{3+} ion is not conducive to improving the luminous intensity, and the slightly higher amount of Bi^{3+} ion doping has the tendency to transfer more energy to Tb^{3+}. This effective energy transfer from Bi^{3+} to Tb^{3+} can increase the luminous intensity. However, due to the aggregation effect of excess Bi^{3+} ions, the distance between the ions becomes smaller, resulting in a concentration quenching phenomenon, which leads to a decrease in luminous intensity.

According to the Eq. **1**[34] for the critical distance between sensitized ions and activated ions, the critical distance between Bi^{3+} and Tb^{3+} can be obtained:

$$R_c=2[3V/(4\pi XN)]^{1/3} \quad (1)$$

Where N is the number of molecules contained in the unit cell, and X is the sum of the critical concentrations of Bi^{3+} and Tb^{3+}. For $LiBa_{0.95-y}BO_3:0.05Tb^{3+},yBi^{3+}$ phosphors, the unit cell volume V=0.298 2 nm^3, N=4, X=0.08. After calculation, the critical distance R_c of the quenching concentration was 1.21 nm. In oxide phosphors, only when the critical distance is less than 0.5 nm, the non-radiative energy transfer will be carried

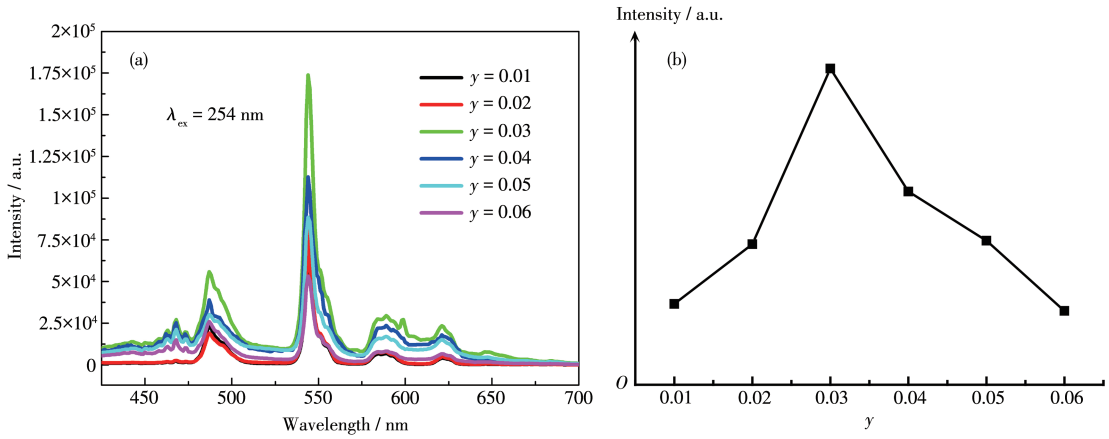

Fig.10 (a) Emission spectra of $LiBa_{0.95-y}BO_3:0.05Tb^{3+},yBi^{3+}$ phosphors; (b) Relative emission intensity as a function of Bi^{3+} concentration for 544 nm peak

out by exchange of interactions. In the $LiBaBO_3$ matrix, the energy transfer between Bi^{3+} and Tb^{3+} is mainly due to multipole-multiple extreme interaction.

For multipole interaction and Reisfeld approximation, the luminous intensity can be calculated according to Dexter′s energy transfer formula (**2**)[35]:

$$\lg(I/y)=c-(\theta/3)\lg y \quad (2)$$

Where I is the luminous intensity of the phosphor $LiBa_{0.95-y}BO_3$：$0.05Tb^{3+}$，yBi^{3+} (y=0.03, 0.04, 0.05, 0.06), y is the concentration of the sensitizing ion Bi^{3+}, c is a constant and θ =6, 8 and 10 correspond to dipole-dipole, dipole-quadrupole, and quadrupole-quadrupole interaction, respectively. The data of the luminous intensity and doping amount of $^5D_4 \rightarrow {}^7F_5$ transition in the phosphors were calculated and fitted, and there was a linear relationship between lg(I/y) and lg y (Fig. 11). After linear fitting, θ was found to be 7.87, and it was closest to 8. Therefore, in $LiBa_{0.95-y}BO_3$：$0.05Tb^{3+}$，yBi^{3+} phosphor, the main energy transfer from Bi^{3+} to Tb^{3+} is through dipole-quadrupole interaction.

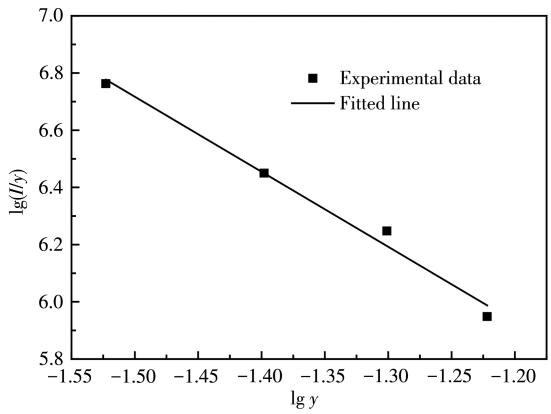

Fig.11　Dependence of lg(I/y) on lg y for $LiBa_{0.95-y}BO_3$：$0.05Tb^{3+}$，yBi^{3+} (y=0.03~0.06) phosphors

2.2.3 CIE color chromaticity coordinates of $LiBa_{0.95-y}BO_3$：$0.05Tb^{3+}$，yBi^{3+}

The CIE color chromaticity coordinates of $LiBa_{0.95-y}BO_3$：$0.05Tb^{3+}$，yBi^{3+} phosphor are shown in Table 2. Fig. 12 shows the chromaticity coordinates of the phosphors that have been marked. It can be observed that when a small amount of sensitizing ion Bi^{3+} was added (y=0.01~0.03), the chromaticity coordinates were mainly located in the green light area. The color change of the powder sample was small, indicating that its luminous performance is relatively stable. When the amount of Bi^{3+} added continued to increase (y =0.04~0.06), the color coordinate position of the phosphor sample was close to the standard ideal white light color coordinate (0.33, 0.33). The overall emission color of the sample showed a gradual trend from green light to white light, which shows that the change of the amount of Bi^{3+} added can adjust the emission color of $LiBa_{0.95-y}BO_3$：$0.05Tb^{3+}$，yBi^{3+} phosphor.

Table 2　Chromaticity coordinates of $LiBa_{0.95-y}BO_3$：$0.05Tb^{3+}$，yBi^{3+} phosphors excited at 254 nm

y	CIE (x, y)
0.01	0.287, 0.510
0.02	0.297, 0.519
0.03	0.298, 0.513
0.04	0.315, 0.424
0.05	0.310, 0.407
0.06	0.302, 0.403

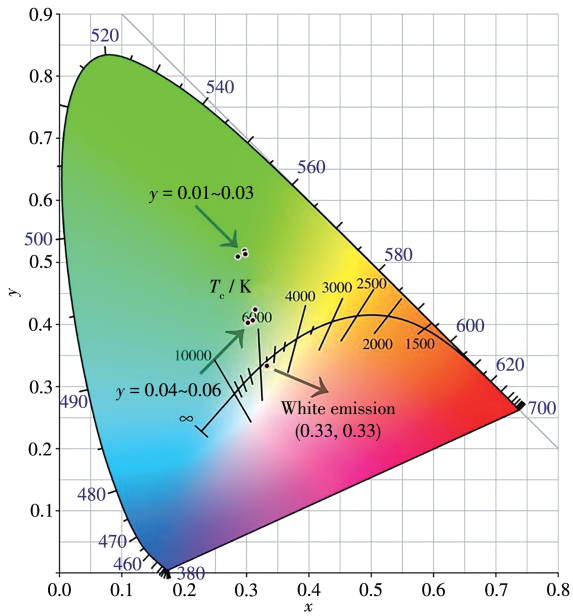

Fig.12　CIE color chromaticity coordinates of $LiBa_{0.95-y}BO_3$：$0.05Tb^{3+}$，yBi^{3+} phosphors

3　Conclusions

A series of Tb^{3+} single-doped phosphors $LiBa_{1-x}BO_3$：xTb^{3+} (x=0.01, 0.02, 0.03, 0.04, 0.05, 0.06, 0.07) were prepared by using traditional high-temperature solid-phase method at not too high temperature. According to the relationship between fluorescent intensity and doping amount of Tb^{3+}, it is found

that the luminous intensity of the product was the largest when x=0.05, so as to determine the optimal doping amount of Tb^{3+}. Another series of phosphor of co-doped Tb^{3+} and Bi^{3+} $LiBa_{0.95-y}BO_3$: $0.05Tb^{3+}$,yBi^{3+} (y=0.01, 0.02, 0.03, 0.04, 0.05, 0.06) were also prepared based on this. The PXRD patterns of two series of phosphors agreed well with $LiBaBO_3$ (PDF No.81-1808), indicating that either single doped Tb^{3+} or co-doped Tb^{3+}/Bi^{3+} did not cause any significant change in the host lattice. $LiBaBO_3$ belongs to the monoclinic crystal system, and the space group is $P2_1/n$. All samples were pure phase, and their microscopic morphology was mainly composed of massive particles and a large number of needle-like crystal grains on the surface, and had good crystallization properties. Fluorescent spectra showed that the luminescent intensities of the second series of phosphors were better than those of the first series, which indicates that Bi^{3+} has a sensitizing effect on the luminescence of Tb^{3+} . The emission intensity initially increased with Bi^{3+} molar fraction, and reached a maximum at molar fraction of Bi^{3+} being 0.03. A decrease in the emission intensity was observed as the Bi^{3+} molar fraction continued to increase, and this shows the occurrence of energy migration between Bi^{3+} and Tb^{3+} ions at different sites in the lattice, resulting in content quenching. CIE color chromaticity coordinates show that the luminescent color of $LiBa_{0.95-y}BO_3$: $0.05Tb^{3+}$, yBi^{3+} presented a gradual trend from green to white, which provides useful information for the preparation and application of such luminescent materials.

References:

[1] Jüstel T, Nikol H, Ronda C. *Angew. Chem. Int. Ed.*, **1998**,**37**(22):3084-3103

[2] Wang X F, Xu J T, Yu J H, Bu Y Y, Marques-Hueso J, Yan X H. *Phys. Chem. Chem. Phys.*, **2020**,**22**(27): 15120-15162

[3] Yu Z F, Eich C, Cruz L J. *Front. Chem.*, **2020**,**8**:496

[4] Sokolnicki J. *J. Lumin.*, **2013**,**134**:600-606

[5] Gordon W O, Carter J A, Tissue B M. *J. Lumin.*, **2004**,**108**(1/2/3/4): 339-342

[6] Goldys E M, Drozdowice-Tomsia K, Sun J J, Dosev D, Kennedy L M, Yatsunenko S, Godlewski M. *J. Am. Chem. Soc.*, **2006**,**128**(45):14498-14505

[7] Saif M, Shebl M, Nabeel A I, Shokry R, Hafez H, Mbarek A, Damak K, Maalej R, Abdel-Mottaleb M S A. *Sens. Actuators B*, **2015**,**220**:162-170

[8] Gai S L, Li C X, Yang P P, Lin J. *Chem. Rev.*, **2014**,**114**(4):2343-2389

[9] Bünzli J C G. *Chem. Rev.*, **2010**,**110**(5):2729-2755

[10]Eiseeva S V, Bünzli J C G. *Chem. Soc. Rev.*, **2010**,**39**(1):189-227

[11]Shen J, Sun L D, Yan C H. *Dalton Trans.*, **2008**,**42**:5687-5697

[12]Feldmann C, Jüstel T, Ronda C R, Schmidt P J. *Adv. Funct. Mater.*, **2003**,**13**(7):511-516

[13]Su X, Yang Z H, Lee M H, Pan S L, Wang Y, Fan X Y, Huang Z J, Zhang B B. *Phys. Chem. Chem. Phys.*, **2015**,**17**(7):5338-5344

[14]Dai W B, Ye S, Li E L, Zhuo P Z, Zhang Q Y. *J. Mater. Chem. C*, **2015**,**3**(31):8132-8141

[15]Yao W J, Xu T, Jiang X X, Huang H W, Wang X Y, Lin Z S, Chen C T. *Dalton Trans.*, **2014**,**43**(26):9998-10004

[16]Müller M, Fischer S, Jüstel T. *RSC Adv.*, **2015**,**5**(83):67979-67987

[17]Sun X R, Gao W L, Cong R H, Yang T. *New J. Chem.*, **2015**,**39**(12): 9886-9893

[18]Zhao D, Ma F X, Zhang R J, Wei W, Yang J, Li Y J. *J. Mater. Sci: Mater. Electron.*, **2017**,**28**(1):129-136

[19]Zheng J H, Cheng Q J, Wu S Q, Zhuang Y X, Guo Z Q, Lu Y J, Chen C. *Mater. Chem. Phys.*, **2015**,**165**:168-176

[20]候晓飞, 赵婉男, 马晶, 孙继强, 李艳红. 无机化学学报, **2020**,**36**(2):276-282
HOU X F, ZHAO W N, MA J, SUN J Q, LI Y H. *Chinese J. Inorg. Chem.*, **2020**,**36**(2):276-282

[21]Zhao J, Huang S X, Zhao D, Huang C H, Ma M J, Zhang R J, Fan Y C, Liu B Z, Gao J W, Zong Q, Yu Y P. *Optik*, **2018**,**159**:115-122

[22]Li P L, Pang L B, Wang Z J, Yang Z P, Guo Q L, Li X. *J. Alloys Compd.*, **2009**,**478**(1/2):813-815

[23]Wang R, Xu J, Chen C. *Mater. Lett.*, **2012**,**68**:307-309

[24]Dillip G R, Mallikarjuna K, Dhoble S J, Raju B D P. *J. Phys. Chem. Solids*, **2014**,**75**(1):8-14

[25]Chen P C, Mo F W, Guan A X, Wang R F, Wang G F, Xia S Y, Zhou L Y. *Appl. Radiat. Isot.*, **2016**,**108**:148-153

[26]Zhang X G, Gong M L. *Ind. Eng. Chem. Res.*, **2015**, **54**(31): 7632-7639

[27]Xin M, Tu D T, Zhu H M, Luo W Q, Liu Z G, Huang P, Li R F, Cao Y G, Chen X Y. *J. Mater. Chem. C*, **2015**,**3**(28):7286-7293

[28]Leng Z H, Yu G H, Li L L Zhang N N, Liu Y L, Gan S C. *J. Alloys Compd.*, **2015**,**651**:679-684

[29]Li P L, Yang Z P, Wang Z J, Guo Q L. *Mater. Lett.*, **2008**,**62**(10/11): 1455-1457

[30]Yawalkar M M, Nair G B, Zade G D, Dhoble S J. *Mater. Chem. Phys.*, **2017**,**189**:136-145

[31]Neharika, Singh V K, Sharma J, Bedyal A K, Kumar V, Swart H C. *J. Alloys Compd.*, **2018**,**738**:97-104

[32]Lephoto M A, Tshabalala K G, Motloung S J, Shaat S K K, Ntwaeaborw O M. *Luminescence*, **2017**,**32**(6):1084-1091

[33]Mo G L, Wei Z, Ma L, Wen G H. *J. Mater. Sci: Mater. Electron.*, **2017**,**28**(3):2557-2562

[34]Blass G. *Philips Res. Rep.*, **1968**,**28**(6):444-445

[35]Li P L, Wang Z J, Yang Z P, Guo Q L, Li X. *Mater. Lett.*, **2009**,**63**(9/10):751-753